Impact of transient groundwater storage on the discharge of Himalayan rivers

Christoff Andermann, Laurent Longuevergne, Stéphane Bonnet, Alain Crave,

Philippe Davy, Richard Gloaguen

HAL Id: hal-00710433
https://hal.archives-ouvertes.fr/hal-00710433

Submitted on 21 Jun 2012

Impact of transient groundwater storage on the discharge of Himalayan rivers

Christoff Andermann[1,2], Laurent Longuevergne[1], Stéphane Bonnet[3], Alain Crave[1], Philippe Davy[1] and Richard Gloaguen[2]

[1] Géosciences Rennes, Université de Rennes 1, CNRS, Campus de Beaulieu, 35042 Rennes, France

[2] Remote Sensing Group, Geology Institute, TU Bergakademie Freiberg, B.-von-Cotta-Str. 2, 09599 Freiberg, Germany

[3] Géosciences Environnement Toulouse, Université de Toulouse, CNRS-UPS-IRD, Observatoire Midi-Pyrénées, 14 Av. Edouard Belin, 31400 Toulouse, France

Corresponding author:

Christoff Andermann,

Tel (+33) 2 23 23 66 24

christoff.andermann@univ-rennes1.fr

The transfer of precipitation into rivers involves temporary water storage in reservoirs[1,2] such as soils, groundwater, snow and glaciers, where different residence times influence the hydrological cycle. In the central Himalayas, the water budget is considered to be primarily controlled by monsoon rainfall, snow and glacier melt[3,4], and secondarily by evapotranspiration[3]. The existence of a deep groundwater contribution[5-7] is deduced from the chemistry of Himalayan rivers[6]. However, its importance in the annual water budget remains to be evaluated. Here, we analyze ~30 years of daily precipitation and discharge within major catchments in Nepal. We observe annual precipitation-discharge hysteresis loops, in both glaciated and unglaciated catchments, independently of the geological setting. This implies the temporal storage of water in

27 **a reservoir whose characteristic response time (~45 days) represents a typical diffusivity (~1 m² s⁻**

28 **¹) of fractured basement aquifers[8]. This transient storage capacity is of ~28 km³ for the three**

29 **main catchments of Nepal, whereas we estimate snow and glacier melt contribution to be ~14**

30 **km³ yr⁻¹ (~10% of the annual river discharge). We conclude that groundwater storage in**

31 **fractured basement constitutes an important compartment of the Himalayan river discharge**

32 **cycle, that can be quantified through the study of precipitation and discharge throughout the**

33 **year.**

34

35 The discharge of the central Himalayan rivers is governed by a strong precipitation seasonality

36 [3,6,9,10] (Fig. 1) with up to 80% of the annual rainfall occurring during the Indian Summer Monsoon

37 (ISM) season[3]. The ISM precipitation is the main source for glacier mass accumulation[9] and its spatial

38 distribution is strongly influenced by orographic effects[3]. Variations in intensity and duration of the

39 ISM, linked to El Nino/Southern Oscillation (ENSO)[11], enhance the annual amount of precipitation by

40 ~25 to 50% with respect to the annual mean at low to moderate elevation (>3 km), and up to 200% at

41 high elevation[12]. Snowmelt contributes to a significant fraction of river discharge in the western and

42 eastern Himalayas and on the Tibetan plateau[3,13], but only to a minor fraction (~10%) in the central

43 Himalayas, mainly in the early ISM (May to July)[3]. It has been suggested that rainfall-derived

44 discharge, ice and snowmelt are the primary factors controlling Himalayan river discharge, with

45 evapotranspiration forming a secondary minor component[3]. Notwithstanding, this hydrological budget

46 model neglects transient water storage in soils, floodplains and groundwater. However, geochemical

47 data indicate that a non-negligible part of surface runoff originates from deep groundwater reservoirs[6].

48

49 We investigate the transfer of water within the main catchments of the Nepal Himalayas (Fig.

50 1a) using a daily meteorological and hydrological dataset spanning ~30 years (Table 1). We consider

51 the three main catchments of Nepal (Sapta Koshi, Narayani and Karnali basins), some of their

52 tributaries, and three unglaciated small catchments at the front of the Himalayan range (Fig. 1a and

53 Table 1). The main catchments drain the entire Himalayan range of Nepal, from the Tibetan Plateau to

54 the Lesser Himalayas. Most of their headwaters are located on the arid Plateau (Fig. 1a), characterized

55   by a weaker influence of the ISM. The rivers incise bedrock comprising, from north to south, the low-

56   grade Paleozoic-Mesozoic Tethyan Sediment Series, high-grade metamorphic gneisses and migmatites

57   of the High Himalayan Crystalline Series and low-grade Proterozoic sediments of the Lesser

58   Himalayas (Fig. 1c). Most of the data considered here come from outlet stations located to the north of

59   the Siwalik foreland. The annual specific discharge of the studied basins is typically on the order of

60   $\sim10^3$ mm yr^{-1} (Table 1) and their annual hydrograph clearly shows the seasonal impact of the ISM on

61   river discharge, generally peaking in July/August[3,14] (Fig. 1b). Mean annual basin precipitation is 920,

62   1396 and 920 mm yr^{-1} in the Sapta Koshi, Narayani and Karnali catchments, respectively. However,

63   precipitation is spatially heterogeneous (Fig. 1a) and is strongly controlled by orography, reaching a

64   maximum between elevations of 2 to 3 km[15,16]. The upper parts of the catchments are glaciated (Fig.

65   1a), covering between 4 and 15 % of the catchment area (Table 1).

66

67   We calculated mean basin-wide daily precipitation rate and use daily discharge measurements

68   to compute specific water discharge for all the studied drainage basins (see Methods). Plots of daily

69   precipitation vs. specific discharge highlight a considerable scatter within the ~30 year dataset (Fig.

70   2a). However, the chronology of the data exhibits a well-defined annual cycle, showing an increase of

71   discharge with increasing precipitation during pre-ISM (March-May) to ISM (June-September) and a

72   decrease during post-ISM (October-November). The systematic higher discharge for a given

73   precipitation rate during post-ISM compared with pre-ISM is striking. The data consequently shows an

74   annual anticlockwise hysteresis loop (Fig. 2a). A 30-day moving average highlights the temporal

75   consistency of the loop from year to year (Fig. 2a, inset). Data scattering results from inter-annual

76   variability, particularly during post-ISM, as illustrated by comparing the data during a strong or a weak

77   ISM year (see Supplementary Fig. S1). The annual anticlockwise hysteresis loop is observed in all

78   studied basins (Fig. 2b), regardless of the geological units, the presence of glaciers or snow cover

79   (Tab. 1).

80

81   Anticlockwise hysteresis loops imply that precipitation is temporarily stored within the

82   catchments and not transferred directly to the river during pre-ISM and ISM seasons, whereas the

83   storage compartment is drained during post-ISM. Glaciers can be directly ruled out as the main

84   contributor to the observed hysteresis effect because the release of water by glacier or snow melt

85   occurs principally during pre-ISM to ISM season[3,13] (Fig. 3b and S2), which is not consistent with the

86   anticlockwise nature of the hysteresis. Moreover, hysteresis effects are observed in both glaciated and

87   unglaciated catchments (Fig. 2b). As the potential evapotranspiration in the Himalayas reaches a

88   maximum during pre-ISM, in April-May[17] (Fig. 1b), this could qualitatively explain the anticlockwise

89   hysteresis loop. However, it is estimated to account for less than 10% of the overall hydrological

90   budget[3], so this effect plays likely a minor role, mainly because the magnitude of evapotranspiration

91   rapidly decreases with elevation[17]. Consequently, the main mechanism explaining the hysteresis effect

92   is likely a transient storage of water in a groundwater unit during the rising ISM and its post-ISM

93   release.

94

95   To precise the role of groundwater storage on the Himalayan hydrological cycle, we solved the

96   water balance at catchment scale in order to discriminate time response distribution in discharge data

97   and relate it to storage compartments via hydrological modeling. We used a modified version of the

98   conceptual hydrological model GR2M (see Methods), which addresses several physical processes in a

99   simplified, but proven robust, way in a wide range of climatological settings[18]. Because the observed

100   hysteresis effect is a seasonal process, daily modeling of hydrological processes is not the pertinent

101   scale for our purpose (see ref. 19). The large diversity of involved processes, within a wide range of

102   environmental settings, limits the reliability of short-term modeling so we modeled the data at a

103   monthly rather than at a daily scale. Note, that we nevertheless tested daily scale modeling (see

104   Methods and Supplementary Table S1). Modeled daily results are generally similar to monthly ones

105   (Table 1), but the efficiency is however less well described (Table 1 and Supplementary Table S1). The

106   model simulates the catchment response to rainfall in terms of river discharge and incorporates three

107   components (see supplementary figure S3): 1) a snow module based on the HBV approach[20] (see

108   Methods), 2) a fast rain-to-discharge flow related to quick runoff processes, and 3) a slow flow

109   component representing groundwater contribution. This third reservoir retards the rain-discharge

110   response and yields baseflow during dry periods. It is characterized by a response time t_c, defined as

111   the time for a hydrological system to reach equilibrium after the hydraulic head has changed[1]. The

112   model is forced by precipitation, temperature and potential evapotranspiration (see Methods). We

113   calibrated on the logarithm of all the observed daily water discharge to account for the large range of

114   discharges, *i. e.* to apply identical weights to both high and low water stages, and under the constraint

115   that total observed and modeled discharge volumes are identical. The modeling is robust in most

116   catchments: hysteresis loops are confidently reproduced for all catchments (e. g. Supplementary Fig.

117   S4) with Nash-Sutcliffe coefficients of 0.89, 0.91 and 0.92 for Sapta Koshi, Narayani and Karnali

118   basins, respectively (Table 1). The modeling implies a significant storage of water within the slow

119   flow reservoir, with calculated t_c longer than one month (Table 1). Modeled data are in agreement with

120   t_c values derived directly from the fit of baseflow recession curves[21] (see Methods and Table 1). This

121   delay between precipitation and discharge yields baseflow during dry periods and is responsible for

122   the existence of the hysteresis loops. Shorter t_c, associated with a low storage capacity (e.g. 10 days

123   equivalent to 20 times smaller storage capacity), do not allow to reproduce the observed hysteresis

124   loops analytically (see Methods and Supplementary Fig. S5c).

125

126   The nature of the groundwater system controlling the hysteresis effect is provided by its

127   response time t_c. For groundwater systems, t_c is inversely proportional to the hydraulic diffusivity D

128   (transmissivity divided by storage coefficient) and is proportional to the square of the characteristic

129   aquifer scale L_c: $t_c \sim L_c^2 * D^{-1}$ [ref 1]. L_c is the characteristic distance between the aquifer and streams, which

130   is approximately the hillslope length if aquifers are spread homogeneously over the drainage basin.

131   Considering L_c in the range 0.5–5 km and t_c, of ~45 days, equivalent diffusivity values are about ~1 m^2

132   s^{-1}, a typical value of aquifers in fractured rocks[8] (0.01 to 10 m^2 s^{-1}). Recession curve exponents

133   calculated on the falling limb of the post-ISM hydrograph (see Methods) are close to 1, and suggest

134   the contribution of a confined aquifer to discharge[21]. The estimated aquifer storage capacity is ~180

135   mm per unit area, representing ~28 km^3 for the three main catchments of Nepal (Table 1). Modeling

136   also indicates that the annual volume of water flowing through this groundwater system represents

137   ~2/3 of the annual river discharge (Supplementary Table S1). The modeled storage dynamics matches

138   the groundwater table variations observed in dug-wells, e.g. in Jhikhu Khola catchment[22] (Fig. 3c).

139   The ratio between calculated water storage variations (Table 1) and water table depth observed here

140   indicates low porosity values of a few percent. We conclude from low porosity values[23], confined

141   behavior[21] and characteristic diffusivity values[8], that the aquifer is predominantly fractured basement.

142   Average water table variation (total annual storage capacity divided by rock porosity, considering low

143   porosity value) is estimated to a few tens of meters in the studied catchments.

144

145   We show that the very specific climatic regime of Nepal, characterized by distinct long lasting

146   wet and dry seasons and a major increase of precipitation during ISM (Fig. 1b and 3a), is responsible

147   for the recharge of fractured basement aquifers. The aquifers are refilled during ISM and purged in

148   post-ISM, leading to the annual hysteresis effect that we observed. This behavior is observed in all the

149   studied drainage basins, independent of their size, physiographic location or main basement geology

150   (Fig. 1, Table 1 and Supplementary Figure S6). Very little is known in Nepal about the actual aquifer,

151   its physical properties and the relationship with tectonic structures. These appear as critical unknowns

152   to go further into our understanding of deep groundwater influence on the Himalayan hydrological

153   cycle, including water resources and flood hazard as well as on landslide risk due to pore-pressure

154   saturation processes. Finally, it is noticeable that during winter (December to February) the

155   precipitation-discharge graphs (Fig. 2b) show a systematic higher baseflow for glaciated catchments

156   compared to unglaciated ones. Because glaciers represent an additional water storage component in

157   some catchments, this vertical shift of the hysteresis loops of glaciated catchments reveals the

158   contribution of glacial melt (and snow in spring) to river discharge and can be used to quantify it.

159   From this approach (see Methods), the snow and glacier melt contribution to river discharge is

160   estimated to be ~14±7 km^3 yr^{-1} considering the three main catchments in Nepal (Table 1), which

161   accounts for ~10% of annual river discharge. In Nepal, the volume of water flowing through fractured

162   basement aquifer is approximately 6 times higher than the contribution of glacial and snow melt to

163   river discharge.

164

165 **Methods**

166 **Data and data processing**

167 Precipitation is calculated using APHRODITE (Asian Precipitation Highly Resolved Observational

168 Data Integration Towards Evaluation of Water Resources) data (http://www.chikyu.ac.jp/precip/).

169 Here, we use the daily version for monsoon Asia APHRO_MA_V1003R1, with a spatial resolution of

170 $0.25°$ [24]. It is currently the best available dataset for Nepal[10]. We use raw river discharge data provided

171 by the Department of Hydrology and Meteorology of Nepal DHM (see e.g. ref. 14), derived from daily

172 stage readings and calibrated rating curves (no interpolated data are used). Potential evapotranspiration

173 is estimated using an elevation-based model developed for Nepal[17]. Basin-wide snow cover is obtained

174 from MOD10C2 version 5 (http://nsidc.org/data/mod10c2v5.html), with an 8-day temporal and 500m

175 spatial resolution[27]. We used the monthly temperature dataset CRU TS3.0[26], with $0.5°$ gridded

176 resolution. Daily temperature is obtained from linear interpolation.

177 **Baseflow recession analysis**

178 Recession curves have been analyzed for time-series of at least 60 days, where daily rainfall is below

179 potential evapotranspiration and cumulated rainfall < 25 mm for each recession curve. The first 15

180 days of each recession are not considered when fitting the recession model. Both linear and non linear

181 models are fitted to the relationship between river discharge Q and storage S: $Q=aS^b$. Analytically,

182 exponent b changes from 1 when transmissivity is constant over time (most likely for confined or very

183 deep unconfined aquifers) to 2 for unconfined flow[21]. Coefficient a is the inverse of the response time

184 when b~1.

185 The annual snow and glacier melt contribution is estimated from the baseflow offset between glaciated

186 and non-glaciated basins along the discharge axis of the hysteresis plots (Fig. 2b). The scatter of

187 baseflow within unglaciated basins (~5 mm/month) is considered as uncertainty. For the Mt. Everest

188 region (here, Dudh Koshi, station 670), our estimated melt volume (0.6 km^3 yr^{-1}, Tab. 1) is consistent

189 with independent glacier mass-loss estimates, measured on ~10% of the glaciated area using satellite

190 altimetry[30].

191 **Hydrological modeling**

192 We consider parsimonious conceptual models at daily and monthly time scales, GR4J and GR2M

193 (http://www.cemagref.fr/webgr/IndexGB.htm). The initial versions have been built up on 4 and 2

194 parameters respectively. We added a distributed snow module based on the HBV conceptual

195 approach[20]. Data scarcity and requirement of a parsimonious model structure prevented application of

196 a more complex approach. Rainfall and temperature data are redistributed on the ETOPO2v2 (2"

197 resolution) elevation grid. Tsep parameter separates rainfall and snowfall (Supplementary Figure S3).

198 Fusion temperature (T_f) is set to 0°C. Snowmelt (S_m) is driven by a degree-day approach with a

199 constant melting factor M, $S_m=M(T-T_f)$. The snow module adds 2 parameters to the initial GR2M and

200 GR4J models for the whole basin. Modeled snow cover fractions are validated on MODIS snow

201 cover[27] extent ($r^2=0.8$).

202 The modified GR2M is based on 3 storage compartments; the snow storage, soil store and routing

203 store, interpreted as "groundwater storage" (Supplementary Figure S3). Liquid rainfall and snowmelt

204 are partitioned into excess rainfall, actual evapotranspiration, slow percolation and water remaining in

205 the soil store based on a single parameter. Actual ET is driven by potential ET and reservoir water

206 availability. At monthly time scales, the routing store gathers all water and computes discharge. The

207 model discharge calculation was modified on a physical basis to include a-priori linear behavior from

208 recession curve analysis with variable time response X5, Q=R/X5. GR models allow water exchanges

209 with outside the basin (e.g. subsurface flow) computed with parameter X2. A first order estimate of

210 groundwater flux contribution to river discharge is computed tracking water flow from the routing

211 store of GR4J model.

212

213 **Modulation of hysteresis effect: Influence of precipitation undercatch, snow melt, reservoir**

214 **residence time and glacier melt on the shape of hysteresis loops**

215 The shape of the hysteresis curve is used to deduce catchment groundwater storage capacity. Forward

216 modeling studies allow stepwise interpretation of the hysteresis shape with respect to hydrological

217 processes or observation errors, which might have the potential to explain the hysteresis effect. The

218 Rapti catchment (station 360 unglaciated, with no snow) is considered as a reference to test the

219 cumulative impact of several contributions.

220 We tested:

221 1) The effect of a systematic underestimation of precipitation and snow on the shape of the hysteresis

222 loop. Applying 30% of excess rainfall[10] shrinks the hysteresis along the precipitation axis (Fig. S5 a).

223 2) The impact of snow storage and delayed melting contribution to discharge, using GLDAS-NOAH

224 model output[25] as a realistic a priori estimate (100 mm snow per year). Snow melt contribution drags

225 the baseflow upward (in March, April and June) but does not change the general shape of the

226 hysteresis loop (Fig. S5 a).

227 3) The effect of t_c on the shape of hysteresis loops. The decrease of t_c from ~45 to 10 days, and the

228 associated decrease of the storage capacity, does not allow to reproduce the hysteresis loops observed

229 (Fig. S5 c).

230 4) The effect of glacier melt on the shape of hysteresis loops. We considered glacier melt contribution

231 at a constant rate and following a seasonal temperature cycle. It induces a year long vertical shift of the

232 hysteresis curve (increased baseflow), keeping its shape intact (Fig. S5 b).

233

234

235 **References**

236 1. Alley, W.M., Healy, R.W., LaBaugh, J.W. & Reilly, T.E. Flow and storage in groundwater systems.

237 *Science* **296**, 1985-1990 (2002).

238 2. Oki, T. & Kanae, S. Global hydrological cycles and world water resources. *Science* **313**, 1068-1072

239 (2006).

240 3. Bookhagen, B. & Burbank, D.W. Toward a complete Himalayan hydrological budget:

241 Spatiotemporal distribution of snowmelt and rainfall and their impact on river discharge. *J.*

242 *Geophys. Res.* **115**, 1-25 (2010).

243 4. Scherler, D., Bookhagen, B. & Strecker, M.R. Spatially variable response of Himalayan glaciers to

244 climate change affected by debris cover. *Nature Geosci.* **4**, 156-159 (2011).

245   5. Anderson, S.P., Dietrich, W.E. & Brimhall, G.H. Weathering profiles, mass-balance analysis, and
246   rates of solute loss: Linkages between weathering and erosion in a small, steep catchment.
247   *Geol. Soc. of Am. Bull.* **114**, 1143-1158 (2002).

248   6. Tipper, E. et al. The short term climatic sensitivity of carbonate and silicate weathering fluxes:
249   Insight from seasonal variations in river chemistry. *Geochim. Cosmochim. Acta* **70**, 2737-2754
250   (2006).

251   7. Calmels, D. et al. Contribution of deep groundwater to the weathering budget in a rapidly eroding
252   mountain belt, Taiwan. *Earth Planet. Sci. Lett.* **303**, 48-58 (2011).

253   8. Montgomery, D.R. & Manga, M. Streamflow and water well responses to earthquakes. *Science* **300**,
254   2047-2049 (2003).

255   9. Barros, A.P., Chiao, S., Lang, T.J., Burbank, D. & Putkonen, J. From weather to climate-Seasonal
256   and interannual variability of storms and implications for erosion processes in the Himalaya.
257   *Geol. Soc. Am. Spec. Pap.* **2398**, 17–38 (2006).

258   10. Andermann, C., Bonnet, S. & Gloaguen, R. Evaluation of precipitation data sets along the
259   Himalayan front. *Geochem. Geophys. Geosys.* **12**, Q07023 (2011).

260   11. Shrestha, M.L. Interannual variation of summer monsoon rainfall over Nepal and its relation to
261   Southern Oscillation Index. *Meteorol. Atmosph. Physics* **75**, 21-28 (2000).

262   12. Bookhagen, B., Thiede, R. & Strecker, M. Abnormal monsoon years and their control on erosion
263   and sediment flux in the high, arid northwest Himalaya. *Earth Planet. Sci. Let.* **231**, 131-146
264   (2005).

265   13. Immerzeel, W., Droogers, P., Dejong, S. & Bierkens, M. Large-scale monitoring of snow cover and
266   runoff simulation in Himalayan river basins using remote sensing. *Remote Sens. Environ.* **113**,
267   40-49 (2009).

268   14. Hannah, D., Kansakar, S., Gerrard, A. & Rees, G. Flow regimes of Himalayan rivers of Nepal:
269   nature and spatial patterns. *J. Hydrol.* **308**, 18-32 (2005).

270   15. Bookhagen, B. & Burbank, D.W. Topography, relief, and TRMM-derived rainfall variations along
271   the Himalaya. *Geophys. Res. Lett.* **33**, 1-5 (2006).

272   16. Putkonen, J.K. Continuous Snow and Rain Data at 500 to 4400 m Altitude near Annapurna, Nepal,
273   1999–2001. *Arctic, Antarctic, and Alpine Research* **36**, 244-248 (2004).

274   17. Lambert, L. & Chitrakar, B. Variation of potential evapotranspiration with elevation in Nepal.
275   *Mountain Research and Development* **9**, 145–152 (1989).

276   18. Mouelhi, S., Michel, C., Perrin, C. & Andreassian, V. Stepwise development of a two-parameter
277   monthly water balance model. *J. Hydrol.* **318**, 200-214 (2006).

278   19. Wang, Q.J. et al. Monthly versus daily water balance models in simulating monthly runoff. *J.*
279   *Hydrol.* **404**, 166-175 (2011).

280   20. Bergström, S. *The HBV Model. Computer models in watershed hydrology. V. P. Singh ed.***,** 443-476
281   (Water Resources Publications: Colorado, USA, 1995).

282   21. Wittenberg, H. Baseflow recession and recharge as nonlinear storage processes. *Hydrol. Processes*
283   **13**, 715-726 (1999).

284   22. Dongol, B.S. et al. Shallow groundwater in a middle mountrain catchment of Nepal: quantity and
285   quality issues. *Env. Geol.* **49**, 219-229 (2005).

286   23. De Marsily, G. *Quantitative Hydrogeology: Groundwater Hydrology for Engineering*. (Academic
287   Press: Orlando, 1986).

288   24. Yatagai, A. et al. A 44-year daily gridded precipitation dataset for Asia based on a dense network of
289   rain gauges. *Sola* **5**, 137–140 (2009).

290   25. Rodell, M. et al. The Global Land Data Assimilation System. *Bulletin of the American Meteorol.*
291   *Soc.* **85**, 381-394 (2004).

292   26. Mitchell, T.D. & Jones, P.D. An improved method of constructing a database of monthly climate
293   observations and associated high-resolution grids. *Int. J. Clim.* **25**, 693-712 (2005).

294 27. Hall, D.K., Riggs, A.G. & Salomonson, V.V. MODIS/Terra Snow Cover 8-Day L3 Global 0.05deg
295   CMG V005, MOD10C2. Boulder, Colorado USA: National Snow and Ice Data Center. *Digital*
296   *media* (2006 updated daily).

297 28. National Snow and Ice Data Center. World glacier inventory. World Glacier Monitoring Service
298   and National Snow and Ice Data Center/World Data Center for Glaciology, Boulder, CO.
299   Digital media. (1999 updated 2009).

300 29. Department of Mines and Geology Nepal. Geological Map of Nepal. 1:1.000.000 (1994).

301 30. Bolch, T., Pieczonka, T. & Benn, D.I. Multi-decadal mass loss of glaciers in the Everest area
302   (Nepal Himalaya) derived from stereo imagery. *The Cryosphere* **5**, 349-358 (2011).

303

310 **Authors contributions**

311 C.A. acquired and analyzed the data. L.L. and C.A. performed the hydrological modeling. All authors
312 discussed the results and wrote the manuscript.

313 **Additional information**

314 Correspondence and requests for materials should be addressed to C.A.

315

316 **Figure captions**

317 **Figure 1| Hydrological setting of the Nepal Himalayas. a,** Precipitation distribution map,
318 hydrological discharge stations used in this study (black diamonds) and contours (red lines) of the
319 studied drainage basins. Grey lines mark political boundaries. Mean annual precipitation rates (see

320   methods), representing 50 years of data, are draped over shaded relief. River network is displayed in

321   blue and glaciers in white (after ref. 28). **b,** Mean basin-wide precipitation (1951-2006, in green),

322   discharge (blue) and potential evapotranspiration (red) for the Narayani drainage basin. Bold blue line

323   with blue shading represents the mean, maximum and minimum daily discharge over 34 years (station

324   450). **c,** Simplified geological map of Nepal[29]: QS: Quaternary Sediments, SW: Siwaliks formation,

325   LH: metasediments of the Lesser Himalayas, HCC: High Himalayan Cristalline, TSS: Tethyan

326   Sediment Series.

327

328   **Figure 2| Precipitation-discharge (P-Q) anticlockwise hysteresis plot. a,** Bi-logarithmic P-Q plot of

329   daily data for the Narayani basin over 34 years at station 450 (~12,300 data points). Data plotted are

330   specific discharges (discharges normalized by drainage area) and mean basin precipitation rates. Note

331   that discharge is not plotted when precipitation is zero. Color bar is scaled for a calendar year. White

332   filled circles represent the mean monthly values over 34 years, the months being indicated by

333   numbers. The error bars represent the 5% and 95% quantiles of the daily data distribution of each

334   month. Inset shows the data filtered with a 30-day moving average. **b,** Mean annual hysteresis loops

335   plotted from monthly mean data for all the drainage basins. Solid lines represent partially glaciated

336   basins and dashed lines unglaciated ones (percentage of glacial coverage from ref. 28).

337

338   **Figure 3| 10-year (1997-2006) temporal variability of several hydrological compartments,**

339   **Narayani basin**. **a,** Daily precipitation (green), and daily specific river discharge (blue). **b,**

340   Temperature (orange) as a glacier melt proxy (from CRU[26]) and percentage of basin-wide snow cover

341   (dark green, data from MODIS MOD10C2 v.5[27] with a 8-day temporal resolution). **c,** Calculated

342   groundwater storage (red), shading illustrating model uncertainty (Supplementary Figure S2). Ground

343   water table variation (dark blue) observed in a dug-well in Jhikhu Khola Basin[22] (station no. 1) from

344   ref. 22 and unpublished data provided by these authors. The abnormal low water table in 2004 likely

345   results from exhaustive exploitation.

346

347

348 **Table 1| Properties of the studied drainage basins and summary of results (monthly modeling).**

349 Maximum elevation is used as a proxy for snow occurrence during winter (considering winter

350 snowline at ~3000 m asl.[16]). Precipitation rate is computed as a mean basin value. Specific discharge is

351 computed from daily river gauge data. Real-evapotranspiration ETR is computed from our modeling

352 (see Methods). Storage represents the mean annual amplitude of storage variation and its respective

353 uncertainty in km³ and mm respectively (Supplementary Figure S2). t_c is the characteristic basin

354 response time, derived from hydrological modeling or from the recession curve of hydrographs (see

355 Methods). The % glaciated values are calculated using data from ref. 28. Ice melt is the annual

356 volumetric glacier ice melt contribution to the rivers, estimated from the relative baseflow shift in the

357 precipitation-discharge plot (Fig. 2b). % snow-melt is the contribution of snow to discharge (both

358 directly and via the aquifer).

359

360 **Supplementary Figure**

361 **S1| Difference between strong and weak monsoon hysteresis loops.** Precipitation-discharge

362 hysteresis loop for the strong monsoon year 1999 and the weak monsoon year 1997[11] for the Narayani

363 Basin. Data has been filtered with a 5-day moving average to avoid small-scale noise. The amplitude

364 of the hysteresis loop is larger during strong monsoon years compared to weak ones. Q/A is the

365 specific discharge, P is the mean basin precipitation.

366

367 **S2| 10-year (1997-2006) temporal variability of several hydrological discharge cycle**

368 **compartments, Koshi Basin (I) and Karnali Basin (II), central Nepal. a,** Daily precipitation

369 (green), and daily specific river discharge (blue). **b**, Temperature (orange) as a glacier melt proxy

370 (from CRU[26]) and percentage of basin-wide snow cover (dark green, data from MOD10C2 v.5[27] with

371 an 8-day temporal resolution). **c**, Calculated groundwater storage evolution (red) derived from a

372 modified version of the conceptual hydrological model GR2M[18] (see methods), shading illustrating

373 model uncertainty, and ground water table variation (dark blue) observed in dug-wells in the Jhikhu

374 Khola Basin[22] (station no. 1).

375 **Uncertainty estimation:**

376   A Monte-Carlo approach is carried out to quantify the impact of observation data uncertainties on

377   modeled groundwater properties (storage capacity, response time, see Table 1). Multiplicative errors

378   have been considered for rainfall and discharge. Rainfall might be systematically underestimated by

379   30%[10], and discharge biased by ±5%. Conversely, ET and temperature errors are taken as additive,

380   based on differences between independent datasets. Model is then recalibrated, model structure error is

381   therefore not considered in this uncertainty analysis. While groundwater storage capacity is highly

382   sensitive to systematic bias in precipitation data, recession curves, and therefore time response, are

383   rather well constrained (Table 1).

384

385   **S3| Flowchart of the modified version of the conceptual hydrological model used in this study.**

386   Simplified schema of the conceptual models GR2M and GR4J[18]□, and the added snow module. Black

387   lines applied for both models GR2M and GR4J whereas gray dotted lines applied only for model

388   GR4J. Please refer to Mouelhi et al. 2006 (ref. 18□), the method section and the following web

389   resource http://www.cemagref.fr/webgr/Modelesgb/descriptionsgb.htm for more detailed information.

390

391   **S4| Modeled vs. observed hysteresis loop for Narayani catchment (450).** Data are plotted on a

392   monthly scale. The inset shows the linear correlation between the observed and modeled discharge.

393   Q/A is the specific discharge. P is the monthly basin-wide precipitation rate.

394

395   **S 5| Influence of precipitation undercatch, snow melt, reservoir residence time and glacier melt**

396   **on the shape of hysteresis loops.** The months are indicated by numbers. In all the examples, the mean

397   monthly precipitation-discharge values for Rapti River at station 360 are used as a reference (blue). **a,**

398   Effect of a constant 30% undercatch of precipitation and impact of snowmelt contribution, considering

399   an annual water equivalent of the snowmelt contribution after the GLDAS-NOAH model[25] (inset). **b,**

400   Impact of the basin-wide storage capacity on the hysteresis shape of the Rapti catchment, considering

401   characteristic basin response times of 35 days and of only 10 days, corresponding to a 20-fold

402   downsizing of the storage capacity (see Methods). **c,** Influence of a 100 mm yr^{-1} glacier melt

403 contribution (or storage), considering a constant melt rate, equally distributed over the whole year or

404 assuming a cyclic, temperature-driven ice melt contribution (both illustrated in the inset).
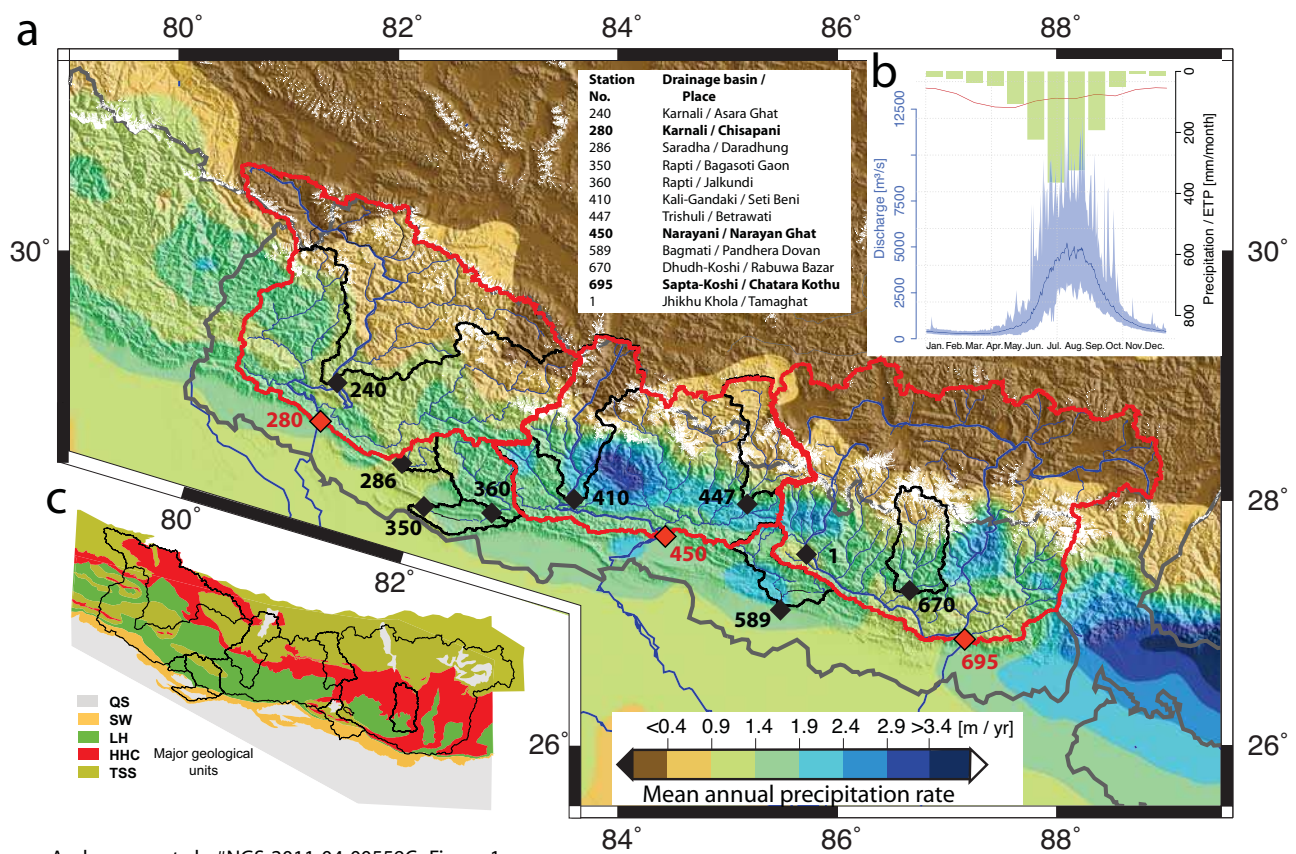
405

406 **S6 | Comparison between groundwater storage properties and geological units within the studied**

407 **drainage basins.** Graphs illustrate storage properties (response time and storage capacity), plotted

408 against geological unites.

409

410 **Table S1| Properties of the studied drainage basins and summary of results (daily modeling)**.

411 Real-evapotranspiration ETR, is computed from the conceptual model GR4J[18] on the basis of potential

412 evapotranspiration[17]. The storage represents the mean annual amplitude of storage variation and its

413 respective uncertainty (Supplementary Figure S2), in km³ and mm respectively. t_c is the characteristic

414 basin response time derived from the model GR4J and the recession curve of the falling limp of the

415 hydrographs. % snow-melt is the contribution of snow to discharge (both directly and via the aquifer).

416 The retarded discharge represents groundwater contribution to the river discharge and is expressed as

417 percent   of   the   annual   river   discharge.

a

Station No.	Drainage basin / Place
240	Karnali / Asara Ghat
280	**Karnali / Chisapani**
286	Saradha / Daradhung
350	Rapti / Bagasoti Gaon
360	Rapti / Jalkundi
410	Kali-Gandaki / Seti Beni
447	Trishuli / Betrawati
450	**Narayani / Narayan Ghat**
589	Bagmati / Pandhera Dovan
670	Dhudh-Koshi / Rabuwa Bazar
695	**Sapta-Koshi / Chatara Kothu**
1	Jhikhu Khola / Tamaghat

b

c

Major geological units
QS
SW
LH
HHC
TSS

<0.4 0.9 1.4 1.9 2.4 2.9 >3.4 [m / yr]
Mean annual precipitation rate

Andermann et al., #NGS-2011-04-00559C, Figure 1
Two columns, 170 mm large

a

b
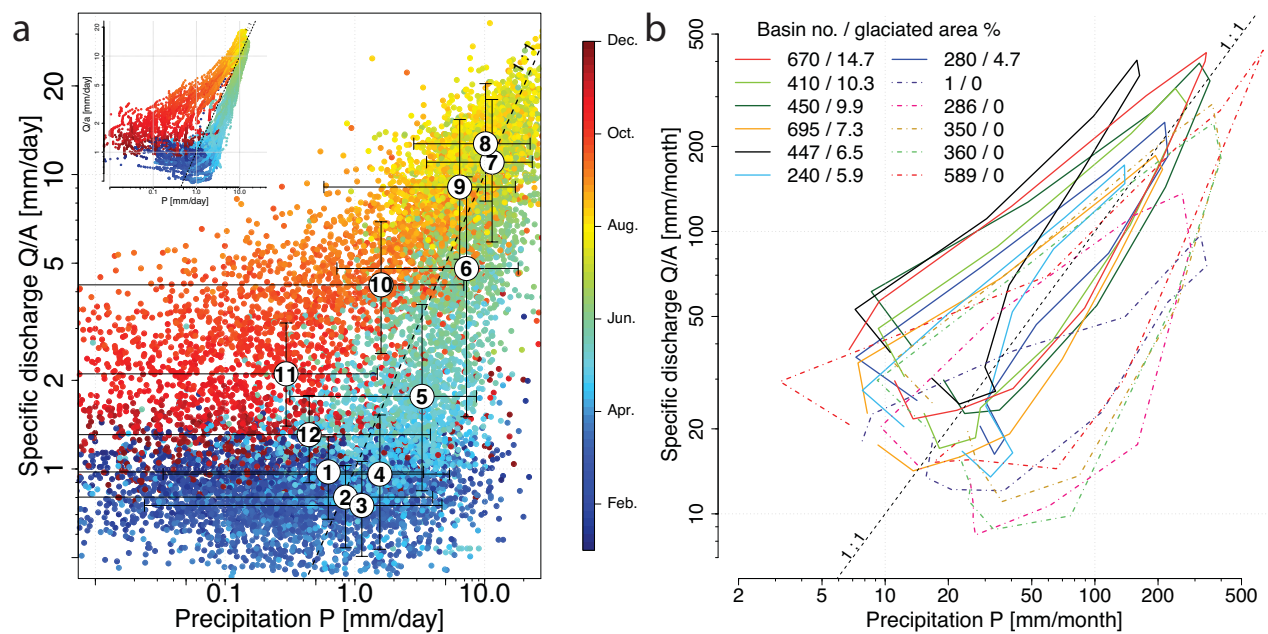
Andermann et al., #NGS-2011-04-00559C, Figure 2
Two columns, 170 mm large
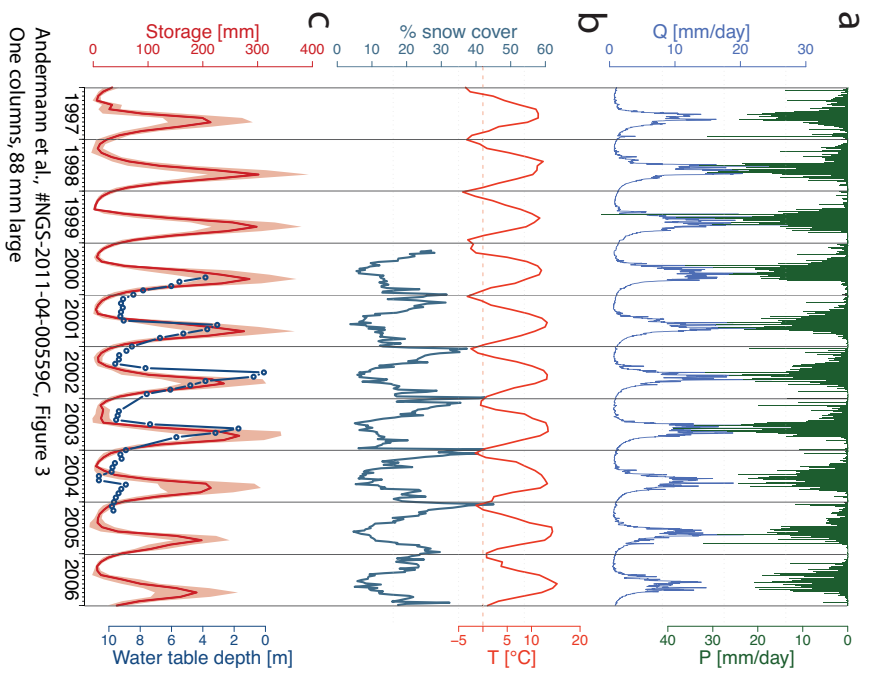
Station No.	240	280	286	350	360	410	447	450	670	695	589	1
Basin	Karnali	**Karnali**	Saradha	Rapti	Rapti	Kali Gandaki	Trishuli	**Narayani**	Dudh Koshi	**Sapta Koshi**	Bagmati	Jhikhu Khola
Lat [°]	28.95	**28.64**	28.64	27.90	27.95	28.01	27.97	**27.71**	27.27	**26.87**	27.11	27.59
Long [°]	81.44	**81.29**	82.03	82.85	82.23	83.60	85.18	**84.43**	86.66	**87.16**	85.48	85.67
Size [km²]	21121	**45967**	808	3648	5198	7169	4428	**32002**	3880	**57719**	2849	111
Precipitation [mm yr⁻¹]	558	**920**	1107	1522	1470	1030	692	**1396**	1295	**920**	1932	1285
Discharge [mm yr⁻¹]	650	**789**	460	903	787	1145	1513	**1145**	1598	**1039**	1205	374
ETR [mm yr⁻¹]	176	**234**	656	720	654	178	121	**367**	178	**179**	839	171
Availability of discharge	1975-2006	**1973-2006**	1976-2006	1978-2006	1985-2006	1979-1995	1977-2006	**1973-2006**	1987-2006	**1977-2006**	2001-2006	1998-2006
%Area glaciated	5.9	**4.7**	0.0	0.0	0.0	10.3	6.5	**9.9**	14.7	**7.3**	0.0	0.0
Max Elevation [m asl.]	7549	**7697**	2800	3623	3623	8147	7352	**8147**	8848	**8848**	2795	2200
Nash-Sutcliffe coef.	0.93	**0.92**	0.79	0.88	0.95	0.91	0.79	**0.91**	0.94	**0.89**	0.88	0.29
Recession exp. b (Q=aS^b)*	1.01	**1.11**	1.16	1.01	1.18	1.01	1.02	**1.16**	1.17	**1.01**	1.12	1.18
Storage capacity [km³]	3.1 ±1.2	**8.1 ±3.3**	0.21 ±0.08	1.6 ±0.7	1.8 ±0.8	1.3 ±0.6	0.9 ±0.4	**9.9 ±3**	1.2 ±0.4	**10.3 ±6**	1.2 ±0.5	0.03 ±0.01
Storage capacity [mm]	150±60	**175±70**	260±90	430±180	350±150	180±80	200±80	**310±125**	300±105	**180±100**	440±180	300±120
t_c GR2M [days]*	46 ±5	**50 ±5**	37 ±3	36 ±8	41 ±8	45 ±4	38 ±4	**50 ±5**	53 ±11	**47 ±4**	30 ±5	120 ±35
t_c recession curve [days]*	40 ±10	**46 ±15**	37 ±13	44 ±17	42 ±15	41 ±15	44 ±11	**40 ±13**	45 ±9	**41 ±11**	41 ±19	77 ±24
Ice+snow melt [km³ yr⁻¹]	1.2	**4.1**	n.a.	n.a.	n.a.	0.7	0.8	**5.3**	0.6	**4.1**	n.a.	n.a.
% snow-melt	12	**7**	n.a.	n.a.	n.a.	3	13	**2**	6	**5**	n.a.	n.a.
Geology units % coverage QS/SW/LH/HHC/TSS	0/0/17/44/39	**0/5/33/25/37**	0/3/96/0/1	0/5/62/0/33	8/24/45/0/23	10/0/32/15/43	0/0/8/37/55	**2/0/42/23/33**	0/0/26/73/1	**6/0/16/40/38**	13/42/2/11/32	0/0/11/17/72

* see Methods